

Low Thermal Crosstalk 808-nm VCSEL Arrays With Nonlinear Mesa Configuration

Volume 10, Number 06, December 2018

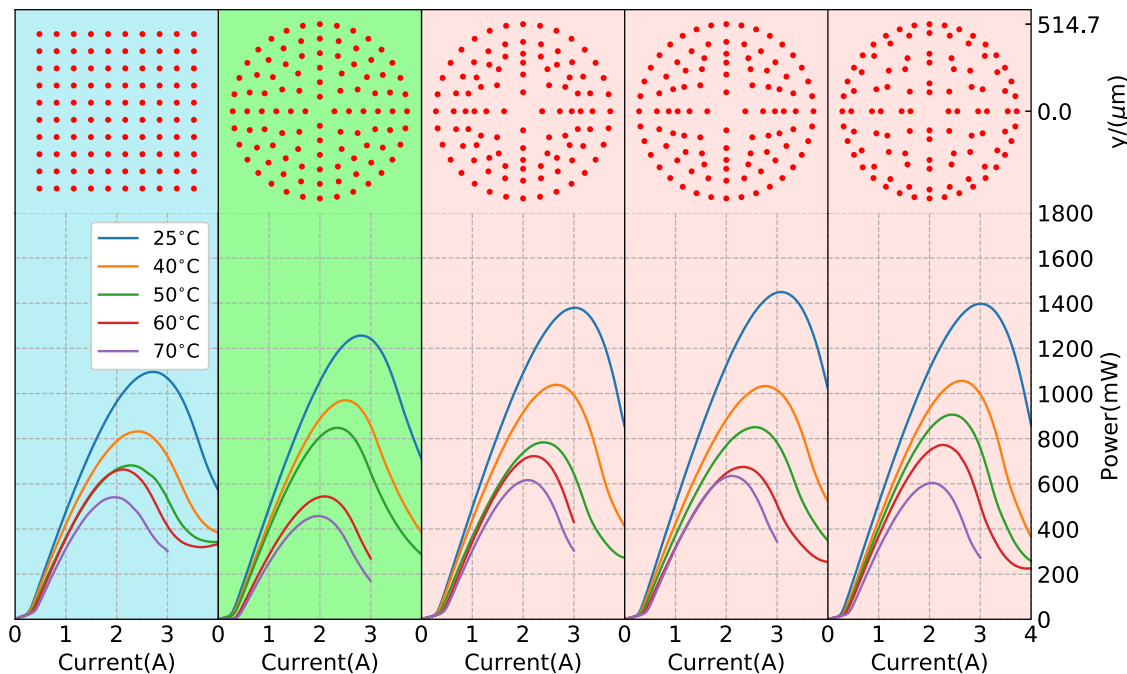
Chuyu Zhong

Xing Zhang, *Member, IEEE*

Werner Hofmann, *Member, IEEE*

Yongqiang Ning

Lijun Wang



DOI: 10.1109/JPHOT.2018.2876694

1943-0655 © 2018 IEEE

Low Thermal Crosstalk 808-nm VCSEL Arrays With Nonlinear Mesa Configuration

Chuyu Zhong ,^{1,2} Xing Zhang ,¹ Member, IEEE,
Werner Hofmann ,³ Member, IEEE,
Yongqiang Ning,¹ and Lijun Wang¹

¹State Key Laboratory of Luminescence and Applications, Changchun Institute of Optics, Fine Mechanics and Physics, Changchun 130033, China

²University of Chinese Academy of Sciences, Beijing 100049, China

³Institut für Festkörperphysik und Zentrum für Nanophotonik, Technical University of Berlin, Berlin 10623, Germany

DOI:10.1109/JPHOT.2018.2876694

1943-0655 © 2018 IEEE. Translations and content mining are permitted for academic research only.
Personal use is also permitted, but republication/redistribution requires IEEE permission.
See http://www.ieee.org/publications_standards/publications/rights/index.html for more information.

Manuscript received September 8, 2018; revised October 4, 2018; accepted October 15, 2018. Date of publication October 18, 2018; date of current version November 5, 2018. This research was supported in part by the National Key Research and Development Program under Grant 2016YFE0126800, in part by the National Natural Science Foundation of China under Grants 61434005, 11774343, 11674314, and 61727822, in part by the Science and Technology Program of Jilin Province, China, under Grant 20160203013GX, in part by the Youth Innovation Promotion Association of China under Grant 2017260, in part by Jilin Scientific and Technological Development Program under Grant 20160204073GX, and in part by Chinese Academy of Sciences President's International Fellowship Initiative under Grant 2018VTA0005. Corresponding author: Xing Zhang (e-mail: zhangx@ciomp.ac.cn).

Abstract: In this paper, we demonstrated vertical-cavity surface-emitting laser (VCSEL) arrays with improved thermal stability by arranging the mesa distribution within the array in a nonlinear configuration. Based on our traversal design algorithm, VCSEL arrays with inhomogeneous mesa-distances were realized. The effects of this rearrangement of mesas on the VCSEL array's thermal stability were studied experimentally. Power-current characteristics and spectra of the 808 nm VCSEL arrays with different mesa distributions were obtained under different thermal stresses in which the optimized devices showed improved performance. The experimental results prove that our algorithm-based optimization is instructive for VCSEL array design.

Index Terms: VCSEL array, mesa distribution, optimization algorithm, thermal stability.

1. Introduction

Vertical-Cavity surface-emitting lasers (VCSELs) have some natural advantages such as symmetrical laser beam and simple integration in two dimensional arrays, making them attractive laser sources for wide range of applications in 3D sensing, optical interconnect, free space communications, laser pumping, illumination or wide-gamut displays [1]–[7]. All of these applications demand devices with high reliability [8], [9] being closely related to thermal stability. Moreover, the lifetime of VCSELs decreases exponentially with rising temperature and excessive heat in active region can do harm to the VCSEL array's performance.

Many efforts have been made to investigate the thermal issue of the VCSEL. Electrical and thermo-electric methods [10]–[13] were developed to analyze the electrical, thermo-physical, and radiative properties of solitary VCSEL devices, which provided valuable reference both theoretically and experimentally. Meanwhile, efforts have also been made for VCSEL arrays. Heat flow in VCSEL

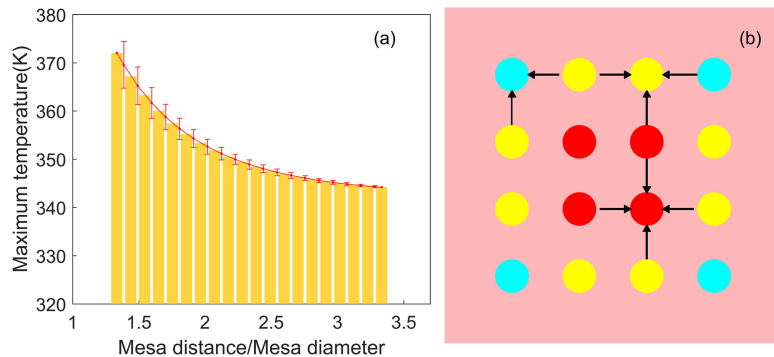


Fig. 1. (a) Maximum temperature for a square VCSEL arrays with different mesa distances ranging from approximately 1.3 to 3.4 times the size of the mesa diameter. Error bars represent the difference between two adjacent columns. (b) Illustrative interaction among different types of mesas. Sky-blue: corner type, yellow: edge type, red: central type.

arrays was simulated with an elongated rectangle shaped VCSEL array predicted to achieve higher power [14]. Effects of oxide-aperture and substrate thickness had been investigated [15].

To reduce thermal influence on VCSELs, using cooling equipment [8] is the most straightforward way and optimization of epitaxial design, material growth, device fabrication and package is always essential [16]. Substrate removal [17] can directly eliminate one of the heat sources and make heat transfer to the heatsink more efficient. Plated copper heatsink on the mesa surface [18] and flip-chip design [19] were adopted to dissipate heat from another side. High contrast grating as top mirror can help cut down heat generation [20]. However, mesa distribution, a factor proved to be effective by our previous research [21] was usually neglected. We designed the mesa distribution to manipulate the interplay of heat flux among mesas and thus temperatures distribution and consequently the array device's performance. Such design can be a supplement to any other methods with no conflict.

In this study, we continue that work and put forward an algorithmic method to design the mesa distribution of VCSEL array quantitatively. Based on the temperature distribution equation of an equal-mesa-distance array, a nonlinear optimization by a rearrangement algorithm was developed to find the optimal mesa distribution. Effects of this optimization on VCSEL array's thermal stability were investigated experimentally. L-I characteristics of the optimized arrays under different heat sink temperatures were compared to normal square array and equal-mesa-loop-distance array. Furthermore, we studied the central wavelength shift of different arrays to indicate that thermal behaviors of various arrays differ. The performance of our optimized arrays is superior compared to our reference devices.

2. Theory and Algorithm of the Rearrangement

Intuitively speaking, arrays with larger mesa-distance can suffer less thermal crosstalk among mesas. However, an over-large distance would make mesas interact weakly to each other and heat crosstalk would become insignificant so the temperature curve became smooth when mesa-distance is large enough as depicted in Fig. 1(a) [21]. Furthermore, mesas near the center interact more with the surrounding mesas thus leading to stronger thermal crosstalk as illustrated in Fig. 1(b). Therefore, the design of distribution of mesas must be dependent on the array size and focus on sufficient mesa-distances.

2.1 Temperature Distribution in an Equal-Mesa-Distance Array

A valid model [22] was built to obtain temperature distribution of an VCSEL array where each mesa dissipates the power P as disk heat source on top of a homogeneous heat sink with a thermal

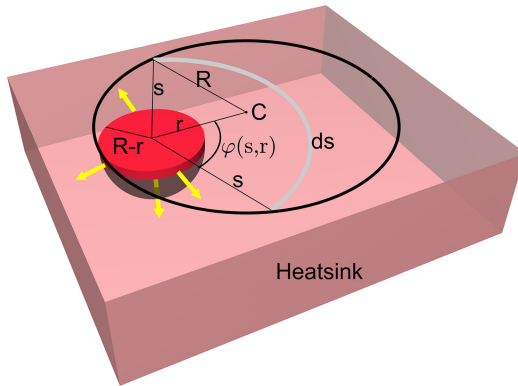


Fig. 2. Integration path of equation (2): C is the center of the disk-shaped array. The point of interest is at distance r from the center. The radius of the whole array is R . We integrate the small red circle first and then the remaining area.

conductivity k . In the model, the array is defined approximately circular-shaped with a radius being R and the pitch of the array being d , as depicted in Fig. 2. The thermal distribution $\Delta T_i(s)$ at the surface or on the active layer of the device caused by a single VCSEL is

$$\Delta T_i(s) = \frac{P}{k} \int_s^\infty \frac{dr}{2\pi r^2} = \frac{P}{2\pi ks} \quad (1)$$

Secondly, all the thermal contributions for an arbitrary VCSEL of the array caused by the other mesas yielding the thermal distribution of the array $\Delta T(r)$ is integrated. Precisely, $\Delta T(r)$ is the additional temperature at the distance r from the center due to thermal crosstalk among mesas via n-DBR and heatsink. The integration path and variables are given in Fig. 2 and the total distribution is given below.

$$\Delta T(r) = \frac{g}{d^2} \left[\int_0^{R-r} 2\pi \Delta T_i(s) s ds + \int_{R+r}^{R+r} 2\varphi(s, r) \Delta T_i(s) s ds \right] \quad (2)$$

where geometrical factor g was introduced for different types of array pitch(1 for Cartesian and $2/\sqrt{3}$ for hexagonal pitch for example). And g/d^2 is mesa density for the equal-mesa-distance array.

2.2 Algorithm for Optimizing Mesa Distribution

To build an efficient algorithm and considering the discrete distribution of mesas in the VCSEL array, a certain level of simplification is required. Firstly, as the mesas are distributed discretely, we need to modify the continuous integral (2) to a summation. Secondly, we remove the g/d^2 factor because the mesa distance should not be fixed in our approach and the absolute value of temperature is not of the priority as we only need to compare the difference of different arrays brought by the mesa distribution. We get

$$\begin{aligned} \Delta T(r) &= \sum_{0 < s < R-r} 2\pi s \cdot \Delta T_i(s) + \sum_{R-r < s < R+r} 2\varphi(s, r) \Delta T_i(s) s \\ &= \sum dS_1 \cdot \Delta T_i(s) + dS_2 \cdot \Delta T_i(s) \end{aligned} \quad (3)$$

where $\Delta T_i(s)$ is proportional to the reciprocal of mesa distance. Omitting all the constants, we can finally define a very simple heat-coupling factor as below

$$H_c = S \sum_{0 < d_i < d_l} \frac{1}{d_i} \quad (4)$$

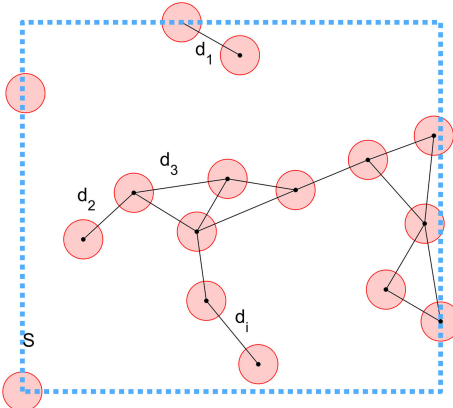


Fig. 3. Illustration of a VCSEL array with randomly distributed mesas. The pink circle represents a mesa; the solid black lines indicate the mesa distance; the area of blue-dashed-line rectangle is S ; the outer square represents the edge of the VCSEL array.

where S is the area including all mesas in the array, d_i is the central distance of each mesa as depicted in Fig. 3 and d_i is the distance limitation only smaller than which the d_i would be included in the summation. Every array has its own H_c value and as a representation of temperature, H_c should be as small as possible. In the same time, the physical meaning of H_c coincides well with our goal. Larger spacing between mesas distance will help reduce thermal interaction, but the size of the array should also be controlled instead of increasing the mesa distance infinitely. Therefore, a product of summation of reciprocal mesa-distances and the whole device's area perfectly satisfies this requirement. By calculating the H_c for each kind of mesa distribution using (4), the algorithm is able to select a mesa distribution with a minimal H_c , in which the mesa distance and whole device's area reach a balance. Based on the meaning above, we would rather define H_c as a dimensionless parameter although it has a unit of length in equation (4).

Heat transferring in the heatsink is almost isotropic, so the shape of the array should be designed as a central symmetric one which meanwhile can largely simplify our algorithm. Therefore, we define the array as loops of mesas. This is a general definition which includes most commonly seen equal-mesa-distance hexagonal or square VCSEL array. In such definition, all the parameters we need to consider are the quantity of loops, distances between loops(or radial positions of loops) and number of mesas in each loop. Since we should control the size of the array, a limitation of the array's radius R would be defined. Hence, our algorithm is developed as a traversal algorithm where all possible combinations of loop-positions will be traversed as shown in Fig. 4(a). The possible radius of each loop range from 0 to R and the step is the mesa radius R_{mesa} because the temperature variance is small within a radius' space [21]. Hence, there are approximately $N_{total} = R/R_{mesa} - 1$ radial positions where N_{loop} loops can be. Therefore there are totally $C_{N_{total}}^{N_{loop}}$ types of mesa distribution with fixed number of mesa-loops and mesas in a loop.

By calculating H_c of each possible array and making comparison at the end, an optimized array with minimal H_c can be chosen. The number of mesas in each loop is not necessarily traversed because there are only a few combinations that can be adopted.

2.3 Array Rearrangement by the Algorithm

To investigate the feasibility of our algorithm, array with 100 mesas is to be designed. According to our simulation result in Fig. 1(a), d_i should be at least three times the size of the mesa diameter. We choose two d_i values and two sets of mesa numbers in different loops and get three types of rearranged VCSEL arrays as shown in Fig. 5. Using $d_i = 6 \times R_{mesa} = 105 \mu\text{m}$ and $N_{mesa} = \{4, 8, 12, 20, 24, 32\}$ in each loop, we obtain array-1 with $R_{loop} = \{112.2, 217.2, 287.2, 339.7, 409.7, 514.7\} \mu\text{m}$ as depicted in Fig. 5(b). Using $d_i = 6 \times R_{mesa} = 105 \mu\text{m}$, $N_{mesa} = \{4, 8, 12, 16, 24, 36\}$ and

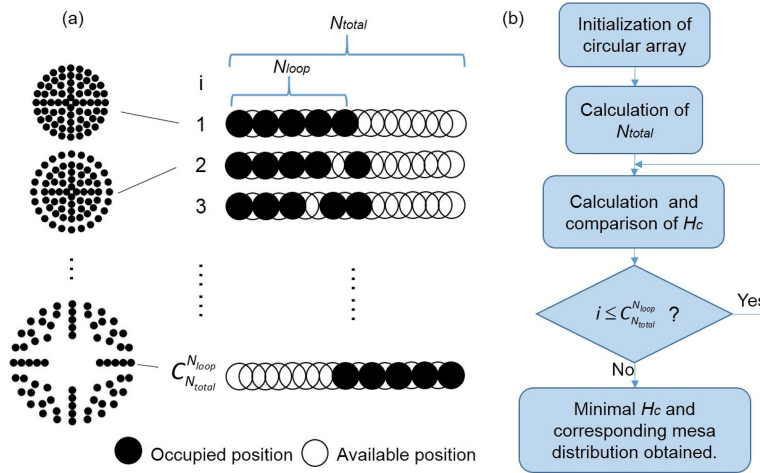


Fig. 4. (a) Schematic illustration and (b) flow chart of the traversal optimization algorithm.

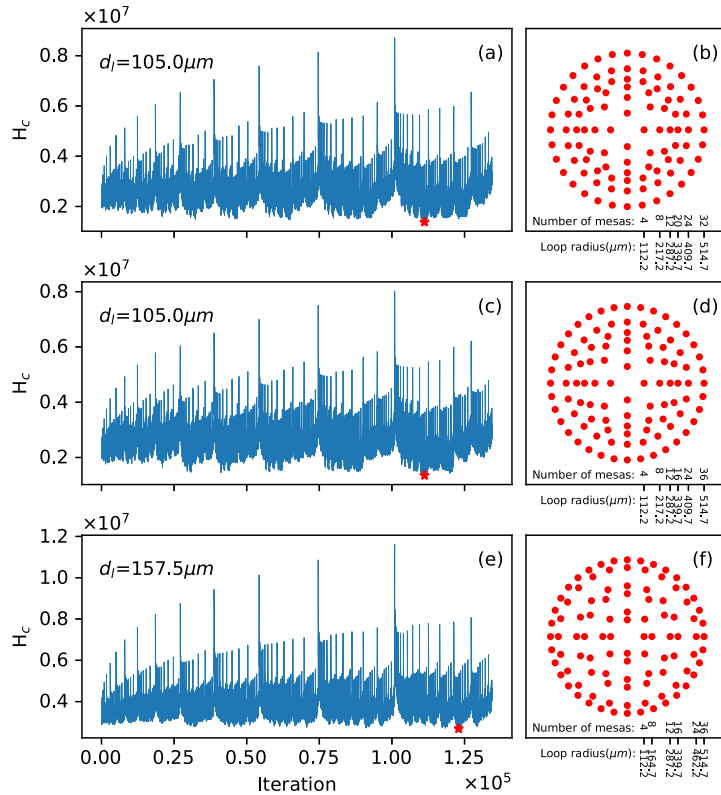


Fig. 5. Calculation processes and VCSEL arrays with minimal H_c using different parameters. (a) (b) H_c curve and optimized array for $d_l = 105 \mu\text{m}$ and $N_{mesa} = \{4, 8, 12, 20, 24, 32\}$. (c) (d) H_c curve and optimized array for $d_l = 105 \mu\text{m}$ and $N_{mesa} = \{4, 8, 12, 16, 24, 36\}$. (e) (f) H_c curve and optimized array for $d_l = 157.5 \mu\text{m}$ and $N_{mesa} = \{4, 8, 12, 16, 24, 36\}$. Minimal H_c s are marked as red stars. The mesa diameter is 35 μm .

using $d_l = 9 \times R_{mesa} = 157.5 \mu\text{m}$, $N_{mesa} = \{4, 8, 12, 16, 24, 36\}$, array-2 with $R_{loop} = \{112.2, 217.2, 287.2, 339.7, 409.7, 514.7\} \mu\text{m}$ and array-3 with $R_{loop} = \{112.2, 164.7, 287.2, 339.7, 462.2, 514.7\} \mu\text{m}$ were obtained as illustrated in Fig. 5(d) and Fig. 5(f) respectively. Radius of the most outer loops are all 514.7 μm . The H_c curves for all possible arrays are shown in Fig. 5(a), (c) and

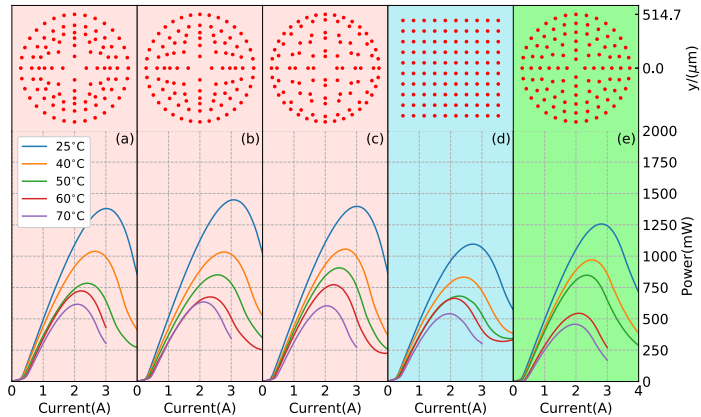


Fig. 6. LI characteristics of (a) array-1, (b) array-2, (c) array-3, (d) square array and (e) ELD array under different heat sink temperatures.

(e) with the minimal H_c s marked as red stars. The H_c values for array-1, 2 and 3 are 1382178.11, 1354205.09 and 2689764.20 respectively.

3. Experiment

Based on the results of our algorithm, we fabricated five kinds of 808 nm top-emitting VCSEL arrays with different mesa distributions, including three optimized arrays, a normal 10×10 square array and an equal-loop-distance circular array (ELD array). To make convective comparison, the S values of all these arrays are the same, which means the mesa spacing in the square array is about $101.4 \mu\text{m}$ and the loop separation in the ELD array is about $85.8 \mu\text{m}$. H_c values of the square array for d_l being $105 \mu\text{m}$ and $157.5 \mu\text{m}$ are 1478036.78 and 2418653.62 respectively. Counterparts of the ELD array are 1721260.04 and 3037413.80 respectively.

All arrays were fabricated on the same wafer with the same mesa diameter of $35 \mu\text{m}$ and oxide aperture of approximately $16 \mu\text{m}$. Firstly mesas were etched by inductively coupled plasma (ICP). Following selective oxidation process, SiO_2 was deposited using plasma enhanced chemical vapor deposition (PECVD). Then the SiO_2 on the top of the mesas is etched away using ICP and the p-contact is formed by DC-sputtered Ti/Pt/Au and lift-off process. The substrate is then thinned down to about $180 \mu\text{m}$ and polished after which n-contact is deposited by sputtering of Ge/Au/Ni/Au. Finally the wafer was split apart and chips were bonded to gold-plated Cu heat sink by In solder.

3.1 LI-Characteristics for Different VCSEL Arrays in Different Heat Sink Temperatures

LI-curves for different arrays in different heat sink temperatures were tested and results are shown in Fig. 6. It could be seen higher outer temperature leads to lower output power, which is caused by additional losses introduced by extra heat. The maximum powers for devices in Fig. 6(a) to (e) under room temperature (25°C) are 1.379 W, 1.449 W, 1.397 W, 1.095 W and 1.256 W respectively. Obviously the performance of optimally designed devices excelled at almost every heat sink temperature.

3.2 Spectra for Different VCSEL Arrays

To further investigate the thermal stability of different types of devices, spectra and wavelength shift were tested. The central wavelength shift (WS) for different devices varied as illustrated in Fig. 7. In favor of our expectation, wavelength shift obeys $WS_{\text{array-2}} < WS_{\text{array-1}} < WS_{\text{array-3}} < WS_{\text{square}} < WS_{\text{ELD}}$. The measured wavelength-temperature variation ($\Delta\lambda/\Delta T$) is 0.07 nm/K [23] so the tem-

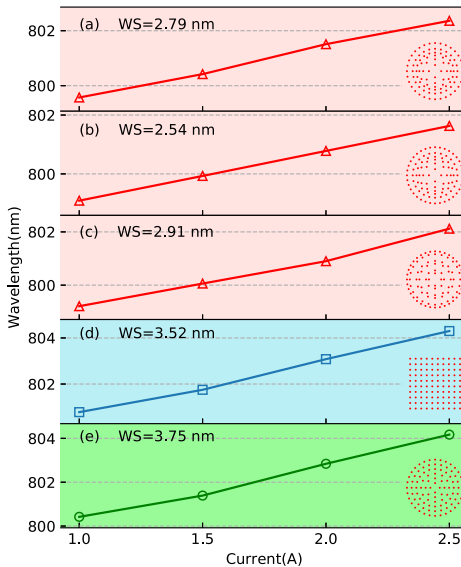


Fig. 7. Central wavelength shift (WS) for (a) array-1, (b) array-2, (c) array-3, (d) square array and (e) ELD array under room temperature.

perature rises from 1 A to 2.5 A injection current for each device are 39.86, 36.29, 41.57, 50.29 and 53.57 K respectively.

4. Conclusion

An algorithm-based optimization of 808nm high-power top-emitting VCSEL array was proposed and experiments were performed. The mesa distribution was rearranged in order to improve the thermal behavior of VCSEL array devices. In the experimental investigation of VCSEL arrays with five kinds of mesa distributions, the optimized VCSEL arrays have shown obvious advantages in LI-characteristics and its thermal stability excels according to the spectra under different driving currents. The distribution of VCSEL mesas has been proven to have an important influence on device performance. Our algorithm efficiently finds the optimal nonlinear device distribution within an array helping to reduce the thermal crosstalk between mesas and strongly improves the devices performance.

References

- [1] K. D. Choquette and J. K. Guenter, Eds., "High-efficiency VCSEL arrays for illumination and sensing in consumer applications," *Proc. SPIE*, vol. 9766, Mar. 2016, Art. no. 97660D.
- [2] A. Kasukawa *et al.*, "Enabling VCSEL technology for 'green' optical interconnect in HPC and data centers," In *Proc. IEEE Photon. Conf.*, 2011, pp. 393–394.
- [3] M. Funabashi *et al.*, "1060nm VCSEL development at Furukawa for parallel optical interconnect," *Proc. SPIE*, vol. 8276, 2012, Art. no. 82760F.
- [4] K. P. Jackson and C. L. Schow, *VCSEL-Based Transceivers for Data Communications*. Berlin, Germany: Springer, 2013, pp. 431–448.
- [5] H. H. Lu *et al.*, "10 m/25 gbps lifi transmission system based on a two-stage injection-locked 680 nm VCSEL transmitter," *Opt. Lett.*, vol. 40, no. 19, pp. 4563–4566, 2015.
- [6] J. F. Seurin *et al.*, "High-brightness pump sources using 2D VCSEL arrays," *Proc. SPIE*, vol. 7615, 2010, Art. no. 76150F.
- [7] Y. Mei *et al.*, "Quantum dot vertical-cavity surface-emitting lasers covering the green gap," *Light: Sci. Appl.*, vol. 6, Jan. 2017, Art. no. e16199.
- [8] J.-F. Seurin *et al.*, "High-power vertical-cavity surface-emitting lasers for solid-state laser pumping," *Proc. SPIE*, vol. 8276, Feb. 2012, Art. no. 827609.

- [9] P. Wolf, P. Moser, G. Larisch, W. Hofmann, and D. Bimberg, "High-speed and temperature-stable, oxide-confined 980-nm VCSELs for optical interconnects," *IEEE J. Sel. Topics Quantum Electron.*, vol. 19, no. 4, Jul. 2013, Art. no. 1701207.
- [10] W. Nakwaski and M. Osinski, "Thermal-properties of etched-well surface-emitting semiconductor-lasers," *IEEE J. Quantum Electron.*, vol. 27, no. 6, pp. 1391–1401, Jun. 1991.
- [11] G. Chen, M. A. Hadley, and J. S. Smith, "Pulsed and continuous-wave thermal-characteristics of external-cavity surface-emitting laser-diodes," *J. Appl. Phys.*, vol. 76, no. 6, pp. 3261–3271, 1994.
- [12] J. Choi, L. Wang, H. Bi, and R. Chen, "Effects of thermal-via structure on thin-film VCSELs for fully embedded board-level optical interconnection system," *IEEE J. Sel. Topics Quantum Electron.*, vol. 12, no. 5, pp. 1060–1065, Sep.–Oct. 2006.
- [13] X. Zhang *et al.*, "A thermal analysis of stable-polarization VCSELs," *Optik*, vol. 157, pp. 203–207, Mar. 2018.
- [14] C. Lei *et al.*, "Design of high power VCSEL arrays," *Proc. SPIE*, vol. 8276, 2012, Art. no. 82760B.
- [15] J. H. Wang, I. Savidis, and E. G. Friedman, "Thermal analysis of oxide-confined VCSEL arrays," *Microelectronics J.*, vol. 42, no. 5, pp. 820–825, 2011.
- [16] D. Zhou *et al.*, "Progress on vertical-cavity surface-emitting laser arrays for infrared illumination applications," *Proc. SPIE*, vol. 9001, Feb. 2014, Art. no. 90010E.
- [17] J. F. Seurin *et al.*, "High-power red VCSEL arrays," *Proc. SPIE*, vol. 8639, 2013, Art. no. 86390O.
- [18] A. Al-Omari, G. Carey, S. Hallstein, J. Watson, G. Dang, and K. Lear, "Low thermal resistance high-speed top-emitting 980-nm VCSELs," *IEEE Photon. Technol. Lett.*, vol. 18, no. 11, pp. 1225–1227, Jun. 2006.
- [19] S. Mishkat-Ui-Masabih, J. Leonard, D. Cohen, S. Nakamura, and D. Feezell, "Techniques to reduce thermal resistance in flip-chip GaN-based VCSELs," *Physica Status Solidi (A)*, vol. 214, no. 8, Jun. 2017, Art. no. 1600819.
- [20] M. As'adi, K. Abbasian, D. A. Bostanabad, and T. Nurmohammadi, "Thermal analysis of high-index-contrast grating (HCG)-based VCSEL," *Optik*, vol. 125, no. 15, pp. 4017–4022, Aug. 2014.
- [21] C.-Y. Zhong, X. Zhang, D. Liu, Y.-Q. Ning, and L.-J. Wang, "Enhanced thermal stability of VCSEL array by thermoelectric analysis-based optimization of mesas distribution," *Chin. Phys. B*, vol. 26, no. 6, 2017, Art. no. 064204.
- [22] M.-C. Amann and W. Hofmann, "INP-based long-wavelength VCSELs and VCSEL arrays," *IEEE J. Sel. Topics Quantum Electron.*, vol. 15, no. 3, pp. 861–868, May–Jun. 2009.
- [23] X. Liang, Y. WANG, L. QIN, T. Li, Y.-Q. NING, and L.-J. WANG, "980nm vertical cavity surface emitting laser temperature-change output characteristics," *Chin. J. Lasers*, vol. 37, no. 1, pp. 87–91, 2010.